
TOWARDS WHOLE PROGRAM GENERATION OF QUADRATURE-FREE DISCONTINUOUS GALERKIN METHODS FOR THE SHALLOW WATER EQUATIONS

A PREPRINT

Sara Faghii-Naini

Department of Computer Science
Friedrich-Alexander-Universität
Erlangen-Nürnberg, Germany
Alfred Wegener Institute
Helmholtz Centre for Polar and Marine Research
Bremerhaven, Germany

Sebastian Kuckuk

Department of Computer Science
Friedrich-Alexander-Universität
Erlangen-Nürnberg, Germany

Vadym Aizinger

Department of Mathematics
Friedrich-Alexander-Universität
Erlangen-Nürnberg, Germany
Alfred Wegener Institute
Helmholtz Centre for Polar and Marine Research
Bremerhaven, Germany

Daniel Zint

Department of Computer Science
Friedrich-Alexander-Universität
Erlangen-Nürnberg, Germany

Roberto Grosso

Department of Computer Science
Friedrich-Alexander-Universität
Erlangen-Nürnberg, Germany

Harald Köstler

Department of Computer Science
Friedrich-Alexander-Universität
Erlangen-Nürnberg, Germany
harald.koestler@fau.de

April 19, 2019

ABSTRACT

The shallow water equations (SWE) are a commonly used model to study tsunamis, tides, and coastal ocean circulation. However, there exist various approaches to discretize and solve them efficiently. Which of them is best for a certain scenario is often not known and, in addition, depends heavily on the used HPC platform. From a simulation software perspective, this places a premium on the ability to adapt easily to different numerical methods and hardware architectures. One solution to this problem is to apply code generation techniques and to express methods and specific hardware-dependent implementations on different levels of abstraction. This allows for a separation of concerns and makes it possible, e.g., to exchange the discretization scheme without having to rewrite all low-level optimized routines manually. In this paper, we show how code for an advanced quadrature-free discontinuous Galerkin (DG) discretized shallow water equation solver can be generated. Here, we follow the multi-layered approach from the ExaStencils project that starts from the continuous problem formulation, moves to the discrete scheme, spells out the numerical algorithms, and, finally, maps to a representation that can be transformed to a distributed memory parallel implementation by our in-house Scala-based source-to-source compiler. Our contributions include: A new quadrature-free discontinuous Galerkin formulation, an extension of the class of supported computational grids, and an extension of our toolchain allowing to evaluate discrete integrals stemming

from the DG discretization implemented in Python. As first results we present the whole toolchain and also demonstrate the convergence of our method for higher order DG discretizations.

Keywords shallow water equations · local discontinuous Galerkin discretization · mixed formulation · quadrature-free · domain specific languages · python · code generation

1 Introduction

ExaStencils¹ provides a multi-layered domain specific language to model various simulation applications in computational science and engineering that involve the solution of partial differential equations (PDEs). It does not rely on other simulation software packages to solve them iteratively but generates the whole simulation program from input data, application parameters, and problem descriptions formulated in an external domain specific language.

In this work, we consider the shallow water equations (SWEs), the main type of model used for prediction of floods caused by tsunami and storm surges as well as for many other problems in oceanography, meteorology, and coastal engineering. We have already shown scalability of a generated basic SWE solver on a GPU cluster [18]. Now we extend our previous work in several directions:

1. apply a state-of-the-art discontinuous Galerkin (DG) method based discretization that we reformulate to become quadrature-free
2. provide a Python interface for our external domain specific language enabling the user to start with a symbolic algebra representation of a discrete problem and transform it automatically to a C++ code via our ExaStencils toolchain
3. add support for more general computational grids necessary for computing more realistic scenarios

Quadrature-free DG discretization: In a quadrature-free DG scheme, all element and face integrals in the discrete formulation are evaluated analytically instead of using quadrature rules. The advantage of a quadrature-free vs. a quadrature integration is the fact that the former eliminates the innermost loop over quadrature points offering thereby a better code optimization potential. This approach is not new (see, e.g., [7, 21]); however, until now, it has mostly been applied to linear problems or problems with product-type nonlinearities (e.g., advection terms in Euler equations) that only involve integrals of polynomials easily evaluated analytically. By exploiting one the main strengths of the local DG (LDG) method, the mixed re-formulation of the original PDEs, we modify the SWE system making it amenable to the quadrature-free methodology in spite of the presence of fraction-type nonlinearities. Whereas, in the original LDG framework [12], such mixed formulations are employed to replace higher-order derivatives by lower-order ones, we took this technique one step further in [10, 2] to handle nonlinearities in the PDE for mean-curvature flow. A similar idea is used in the current work to deal with the fraction terms in the SWE.

Quadrature-free DG formulations are an alternative to the tensor-product DG formulations. Schemes based on the latter approach evaluate multidimensional integrals as products of one-dimensional ones achieving in this way a higher computational intensity particularly for high-order discretizations. While very efficient for element shapes naturally represented in a tensor-product fashion (quads, hexahedra, etc.), this approach is less popular for simplicial elements (triangles, tets), although such generalization also exist (e.g., Dubiner bases [15]).

Other discretization examples for the SWE include a recent DG [32] implementation, finite differences [11, 6] or generalized finite differences [20], or even a mesh-free smoothed particle hydrodynamics (SPH) approach [9]. Efficient implementations are found in literature [33, 23] using, e.g., a quadtree data structure on GPU [30], Sierpinski curves [8], and dynamically adaptive spacetime grids [31]. Some implementations are also running on distributed memory systems [19].

Domain-specific languages for HPC: In addition to software libraries, domain-specific languages (DSLs) also became increasingly prominent in computational science and engineering applications in recent years. A more detailed overview of popular approaches is found in [27]. Particularly relevant ones are Firedrake, STELLA, Mint and SPIRAL. Firedrake [25] is an automated toolchain for solving PDEs specified in a DSL embedded in Python. It employs the unified form language (UFL) [5] and the FEniCS form compiler of the FEniCS project [22]. STELLA [16] targets stencil codes on structured grids and uses, in contrast to ExaStencils, an internal DSL embedded into C++ that is based on template meta programming. Mint [29] is a programming model for GPUs and focuses on the source-to-source compilation of annotated C to CUDA. Finally, SPIRAL [24] provides abstractions for linear transforms and other mathematical functions.

¹<http://www.exastencils.org/>

Our approach builds upon the ExaStencils code generator that relies on an external multi-layered DSL called ExaSlang to map from different levels of abstraction: First, the continuous problem description; next, the discretization; then the numerical algorithm specification; and, finally, a C-like representation of the whole simulation code. The ExaStencils toolchain has been now extended by adding support for a symbolic algebra math-like specification of the discrete problem within Python. The latter is then mapped automatically to the C-like ExaSlang layer, from where a regular code generation process goes on.

Expanding support for more general computational grids: Initially, ExaStencils only supported regular grids with sparse matrix-vector multiplications easily described by stencil operations. In a step-by-step fashion, support for more general computational grids including staggered and grids with locally varying mesh size has been added. In order to be able to run simulations for realistic ocean domain geometries that cannot be accurately approximated by structured grids, our final goal is to support block-structured grids obtained from a coarse unstructured grid refined regularly. To this end, a grid generator is being currently developed to create grids with a block-structured topology as required by the Exastencils framework with first results for complex domains presented in [34].

The paper is structured as follows: In Sec. 2 the continuous problem, its DG discretization, and the algebraic representation of element integrals are described followed by the mapping to executable code via Python and the ExaStencils compiler. Numerical verification of the generated code is presented in Sec. 3.

2 A shallow water equations generator

The main steps of our approach to map a continuous mathematical problem description to an efficient simulation code are sketched in Fig. 1. Next, we describe each of these steps in more detail.

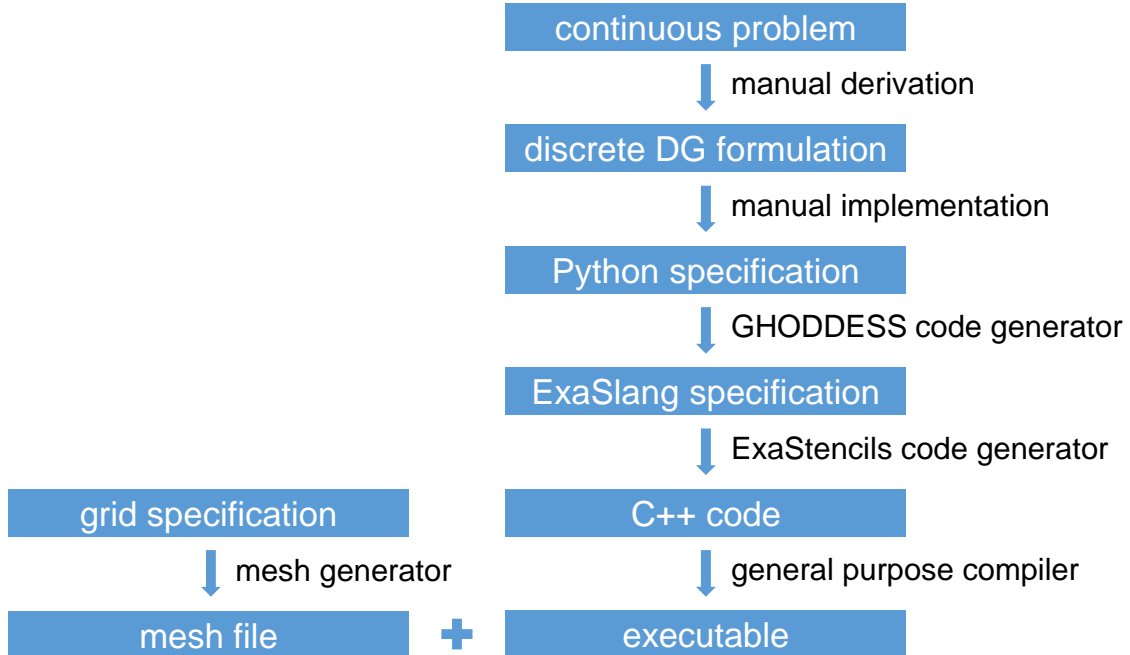


Figure 1: Extended ExaStencils toolchain for generating code for DG discretized SWEs.

2.1 Continuous formulation

The classical 2D SWE are obtained from the vertically integrated Navier-Stokes equations under the additional assumptions of a hydrostatic pressure and a vertically uniform horizontal velocity:

$$\partial_t \xi + \nabla \cdot \mathbf{q} = 0, \quad (1)$$

$$\partial_t \mathbf{q} + \nabla \cdot (\mathbf{q}\mathbf{q}^T / H) + \tau_{bf} \mathbf{q} + \begin{pmatrix} 0 & -f_c \\ f_c & 0 \end{pmatrix} \mathbf{q} + gH \nabla \xi = \mathbf{F}. \quad (2)$$

They are defined on some 2D domain Ω , and ξ represents the elevation of the free water surface with respect to some datum (e.g., the mean sea level). By $H = h_b + \xi$, we denote the total fluid depth with h_b representing the bathymetric depth, $\mathbf{q} \equiv (U, V)^T$ is the depth integrated horizontal velocity field, f_c is the Coriolis coefficient, g is the gravitational acceleration, and τ_{bf} is the bottom friction coefficient. Effects of variable atmospheric pressure, and tidal potentials are expressed through the body force \mathbf{F} .

Defining $\mathbf{c} := (\xi, U, V)^T$ system (1)–(2) is given in the following compact form:

$$\partial_t \mathbf{c} + \nabla \cdot \mathbf{A} = \mathbf{r}(\mathbf{c}), \quad (3)$$

where

$$\mathbf{A} = \begin{pmatrix} U & V \\ \frac{U^2}{H} + \frac{1}{2}g(H^2 - h_b^2) & \frac{UV}{H} \\ \frac{UV}{H} & \frac{V^2}{H} + \frac{1}{2}g(H^2 - h_b^2) \end{pmatrix} \quad (4)$$

and

$$\mathbf{r}(\mathbf{c}) = \begin{pmatrix} 0 \\ -\tau_{bf}U + f_cV + g\xi\partial_x h_b + F_x \\ -\tau_{bf}V - f_cU + g\xi\partial_y h_b + F_y \end{pmatrix}. \quad (5)$$

In the remainder of this paper, the boundary conditions are assumed to be of Dirichlet type; however, a full set of boundary conditions needed for realistic simulations will be included in our implementation in the near future.

2.2 Discretization using a quadrature-free DG method

Our discretization of the SWE system (3) is generally based on the scheme realized in our UTBEST solver [13, 3]. But, instead of a standard quadrature-based evaluation of integrals, we utilize a quadrature-free DG formulation enhanced to deal with nonlinearities in form of fractions. For this purpose, we introduce the depth averaged velocity $\mathbf{u} = (u, v)^T$ given by $\mathbf{q} = \mathbf{u}H$ and extend system (3) by equations for u and v :

$$\partial_t \mathbf{c} + \nabla \cdot \tilde{\mathbf{A}} = \mathbf{r}(\mathbf{c}), \quad (6)$$

$$\mathbf{u}H = \mathbf{q}, \quad (7)$$

where $H^2 - h_b^2 = \xi^2 + 2h_b\xi + h_b^2 - h_b^2 = \xi(H + h_b)$ and thus

$$\tilde{\mathbf{A}} = \begin{pmatrix} U & V \\ Uu + \frac{1}{2}g\xi(H + h_b) & Uv \\ Vu & Vv + \frac{1}{2}g\xi(H + h_b) \end{pmatrix}. \quad (8)$$

Let $\{\mathcal{T}_\Delta\}_{\Delta>0}$ be a family of triangulations of $\Omega \subset \mathbb{R}^2$, and let $\Omega_e, e \in \{0, \dots, E\}$ be elements of \mathcal{T}_Δ . We obtain the variational formulation of system (6)–(7) by multiplication with sufficiently smooth test functions ϕ and ψ and integration by parts on each element $\Omega_e \in \mathcal{T}_\Delta$, which yields:

$$(\partial_t \phi, \phi)_{\Omega_e} - (\tilde{\mathbf{A}}, \nabla \phi)_{\Omega_e} + \langle \tilde{\mathbf{A}} \cdot \mathbf{n}, \nabla \phi \rangle_{\partial\Omega_e} = (\mathbf{r}(\mathbf{c}), \phi)_{\Omega_e}, \quad (9)$$

$$(\mathbf{u}H, \psi)_{\Omega_e} = (\mathbf{q}, \psi)_{\Omega_e}, \quad (10)$$

where $(\cdot, \cdot)_{\Omega_e}$ and $\langle \cdot, \cdot \rangle_{\partial\Omega_e}$ represent the L^2 - scalar products on elements and edges, respectively.

Now denoting by $\mathbb{P}^k(\Omega_e)$ the polynomial spaces of order k on Ω_e , we obtain the discrete formulation using test functions $\phi_\Delta \in \mathbb{P}^k(\Omega_e)^3$, $\psi_\Delta \in \mathbb{P}^k(\Omega_e)^2$:

$$(\partial_t \mathbf{c}_\Delta, \phi_\Delta)_{\Omega_e} - (\tilde{\mathbf{A}}(\mathbf{c}_\Delta, \mathbf{u}_\Delta), \nabla \phi_\Delta)_{\Omega_e} + \langle \hat{\tilde{\mathbf{A}}}(\mathbf{c}_\Delta, \mathbf{u}_\Delta, \mathbf{c}_\Delta^+, \mathbf{u}_\Delta^+, \mathbf{n}), \phi_\Delta \rangle_{\partial\Omega_e} \quad (11)$$

$$= (\mathbf{r}(\mathbf{c}_\Delta, \mathbf{u}_\Delta), \phi_\Delta)_{\Omega_e},$$

$$(\mathbf{u}_\Delta H_\Delta, \psi_\Delta)_{\Omega_e} = (\mathbf{q}_\Delta, \psi_\Delta)_{\Omega_e}, \quad (12)$$

where \mathbf{n} is a unit normal to $\partial\Omega_e$, and $\hat{\tilde{\mathbf{A}}} \cdot \mathbf{n}$ is approximated on $\partial\Omega_e$ by a numerical flux $\hat{\tilde{\mathbf{A}}}(\mathbf{c}_\Delta, \mathbf{u}_\Delta, \mathbf{c}_\Delta^+, \mathbf{u}_\Delta^+, \mathbf{n})$ (here, we utilize the Lax-Friedrichs flux [17]) that depends on discontinuous values of the solution on element Ω_e (without superscript) and on its edge neighbors (superscript $+$). \mathbf{c}_Δ and \mathbf{u}_Δ are the DG approximations to \mathbf{c} and \mathbf{u} and can be represented as

$$\mathbf{c}_\Delta(t, \mathbf{x})|_{\Omega_e} = (\xi_\Delta, U_\Delta, V_\Delta)^T(t, \mathbf{x}) = \sum_{j=1}^3 \sum_{i=1}^{K(k)} c_{ei}^j \varphi_{ei}(\mathbf{x}) \mathbf{e}_j, \quad (13)$$

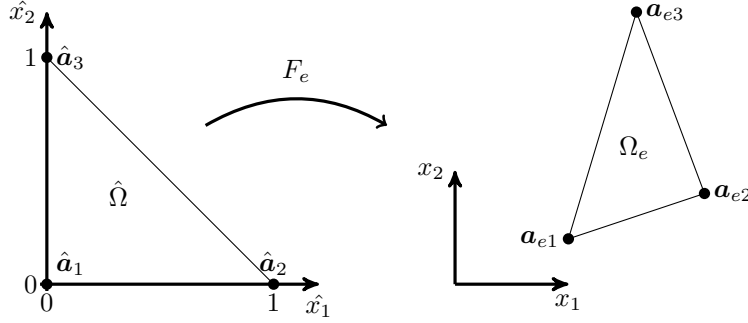


Figure 2: Affine-linear mapping F_e from the reference triangle $\hat{\Omega} = \{\hat{\mathbf{a}}_1, \hat{\mathbf{a}}_2, \hat{\mathbf{a}}_3\} = \{[0, 0]^T, [1, 0]^T, [0, 1]^T\}$ to physical triangle $\Omega_e = \{\mathbf{a}_{e,1}, \mathbf{a}_{e,2}, \mathbf{a}_{e,3}\}$.

$$\mathbf{u}_\Delta(t, \mathbf{x})|_{\Omega_e} = (u_\Delta, v_\Delta)^T(t, \mathbf{x}) = \sum_{j=1}^2 \sum_{i=1}^{K(k)} w_{ei}^j \varphi_{ei}(\mathbf{x}) \mathbf{e}_j \quad (14)$$

with \mathbf{e}_j denoting the j -th unit vector in \mathbb{R}^3 in (13) or \mathbb{R}^2 in (14). A basis of space $\mathbb{P}^k(\Omega_e)$ consisting of $\varphi_{ei}(\mathbf{x})$, $i = 1, \dots, K(k)$ is defined using a mapping from the corresponding reference basis

$$\varphi_{ei}(\mathbf{x}) = \begin{cases} \hat{\varphi}_i(\mathbf{F}_e^{-1}(\mathbf{x})) & \mathbf{x} \in \Omega_e, \\ 0 & \text{otherwise,} \end{cases} \quad i \in \{1, \dots, K(k)\}$$

where $F_e : \hat{\Omega} \rightarrow \Omega_e$, $\hat{\mathbf{x}} \rightarrow \mathbf{x} := \mathbf{B}_e \hat{\mathbf{x}} + \mathbf{a}_{e1}$ is the affine-linear transformation (see Fig. 2) from the reference triangle onto triangle Ω_e with

$$\mathbf{B}_e = \begin{bmatrix} B_{1,1}^e & B_{1,2}^e \\ B_{2,1}^e & B_{2,2}^e \end{bmatrix} := [\mathbf{a}_{e2} - \mathbf{a}_{e1} \quad \mathbf{a}_{e3} - \mathbf{a}_{e1}]$$

and $\mathbf{a}_{e1}, \mathbf{a}_{e2}, \mathbf{a}_{e3}$ denoting the vertex coordinates of Ω_e .

The number of basis functions $K(k)$ is dependent on the respective polynomial space and has the following values: $K(0) = 1$, $K(1) = 3$, $K(2) = 6$, and $K(3) = 10$. The basis functions on the reference triangle $\hat{\Omega}$ employed in our implementation are given by:

$$\left. \begin{array}{l} \hat{\varphi}_1(\hat{\mathbf{x}}) = \sqrt{2}, \\ \hat{\varphi}_2(\hat{\mathbf{x}}) = 2 - 6\hat{x}_1, \\ \hat{\varphi}_3(\hat{\mathbf{x}}) = \sqrt{12}(1 - \hat{x}_1 - 2\hat{x}_2), \\ \hat{\varphi}_4(\hat{\mathbf{x}}) = \sqrt{6}(1 - 8\hat{x}_1 + 10\hat{x}_1^2), \\ \hat{\varphi}_5(\hat{\mathbf{x}}) = \sqrt{3}(-1 - 4\hat{x}_1 + 5\hat{x}_1^2 + 12\hat{x}_2 - 15\hat{x}_2^2), \\ \hat{\varphi}_6(\hat{\mathbf{x}}) = \sqrt{45}(1 - 4\hat{x}_1 + 3\hat{x}_1^2 - 4\hat{x}_2 + 8\hat{x}_1\hat{x}_2 + 3\hat{x}_2^2), \\ \hat{\varphi}_7(\hat{\mathbf{x}}) = \sqrt{8}(-1 + 15\hat{x}_1 - 45\hat{x}_1^2 + 35\hat{x}_1^3), \\ \hat{\varphi}_8(\hat{\mathbf{x}}) = \sqrt{24}(-1 + 13\hat{x}_1 - 33\hat{x}_1^2 + 21\hat{x}_1^3 + 2\hat{x}_2 - 24\hat{x}_1\hat{x}_2 + 42\hat{x}_1^2\hat{x}_2), \\ \hat{\varphi}_9(\hat{\mathbf{x}}) = \sqrt{40}(-1 + 9\hat{x}_1 - 15\hat{x}_1^2 + 7\hat{x}_1^3 + 6\hat{x}_2 - 48\hat{x}_1\hat{x}_2 + 42\hat{x}_1^2\hat{x}_2 - 6\hat{x}_2^2 + 42\hat{x}_1\hat{x}_2^2), \\ \hat{\varphi}_{10}(\hat{\mathbf{x}}) = \sqrt{56}(-1 + 3\hat{x}_1 - 3\hat{x}_1^2 + \hat{x}_1^3 + 12\hat{x}_2 - 24\hat{x}_1\hat{x}_2 + 12\hat{x}_1^2\hat{x}_2 - 30\hat{x}_2^2 + 30\hat{x}_1\hat{x}_2^2 + 20\hat{x}_2^3). \end{array} \right\} \begin{array}{l} \mathbb{P}^0 \\ \mathbb{P}^1 \\ \mathbb{P}^2 \\ \mathbb{P}^3 \end{array}$$

Algebraic representation of element integrals: For compactness, we show an algebraic representation of our discrete scheme only for element integrals. Inserting the basis representations (13), (14) into system (11), (12) and testing the first equation with $\phi_\Delta = \varphi_{ep} \mathbf{e}_1$ we obtain for $p \in 1, \dots, K(k)$:

$$\begin{aligned} \left(\tilde{\mathbf{A}}(\mathbf{c}_\Delta, \mathbf{u}_\Delta), \nabla(\varphi_{ep} \mathbf{e}_1) \right)_{\Omega_e} &= \sum_{l=1}^2 \sum_{i=1}^{K(k)} c_{ei}^{l+1} \int_{\Omega_e} \frac{\partial \varphi_{ep}}{\partial x_l} \varphi_{ei} d\mathbf{x} \\ &= \sum_{i=1}^{K(k)} \left[\frac{c_{ei}^2}{|\det(\mathbf{B}_e)|} \left(B_{2,2}^e \int_{\hat{\Omega}} \frac{\partial \hat{\varphi}_p}{\partial \hat{x}_1} \hat{\varphi}_i d\hat{\mathbf{x}} - B_{2,1}^e \int_{\hat{\Omega}} \frac{\partial \hat{\varphi}_p}{\partial \hat{x}_2} \hat{\varphi}_i d\hat{\mathbf{x}} \right) \right. \\ &\quad \left. + \frac{c_{ei}^3}{|\det(\mathbf{B}_e)|} \left(-B_{1,2}^e \int_{\hat{\Omega}} \frac{\partial \hat{\varphi}_p}{\partial \hat{x}_1} \hat{\varphi}_i d\hat{\mathbf{x}} + B_{1,1}^e \int_{\hat{\Omega}} \frac{\partial \hat{\varphi}_p}{\partial \hat{x}_2} \hat{\varphi}_i d\hat{\mathbf{x}} \right) \right], \end{aligned} \quad (15)$$

For $\phi_\Delta = \varphi_{ep} \mathbf{e}_2$ and $p \in 1, \dots, K(k)$:

$$\begin{aligned}
 \left(\tilde{\mathbf{A}}(\mathbf{c}_\Delta, \mathbf{u}_\Delta), \nabla(\varphi_{ep} \mathbf{e}_2) \right)_{\Omega_e} &= \sum_{j=1}^2 \left[\sum_{i,m=1}^{K(k)} c_{ei}^2 u_{em}^j \int_{\Omega_e} \frac{\partial \varphi_{ep}}{\partial x_j} \varphi_{ei} \varphi_{em} dx \right] \\
 &+ \sum_{i,m=1}^{K(k)} \frac{g}{2} c_{ei}^1 c_{em}^1 \int_{\Omega_e} \frac{\partial \varphi_{ep}}{\partial x_1} \varphi_{ei} \varphi_{em} dx + \sum_{i=1}^{K(k)} g h_b c_{ei}^1 \int_{\Omega_e} \frac{\partial \varphi_{ep}}{\partial x_1} \varphi_{ei} dx \\
 &= \sum_{i,m=1}^{K(k)} \left[\frac{c_{ei}^2 u_{em}^1}{|\det(\mathbf{B}_e)|^{3/2}} \left(B_{2,2}^e \int_{\hat{\Omega}} \frac{\partial \hat{\varphi}_p}{\partial \hat{x}_1} \hat{\varphi}_i \hat{\varphi}_m d\hat{x} - B_{2,1}^e \int_{\hat{\Omega}} \frac{\partial \hat{\varphi}_p}{\partial \hat{x}_2} \hat{\varphi}_i \hat{\varphi}_m d\hat{x} \right) \right. \\
 &+ \left. \frac{c_{ei}^2 u_{em}^2}{|\det(\mathbf{B}_e)|^{3/2}} \left(-B_{1,2}^e \int_{\hat{\Omega}} \frac{\partial \hat{\varphi}_p}{\partial \hat{x}_1} \hat{\varphi}_i \hat{\varphi}_m d\hat{x} + B_{1,1}^e \int_{\hat{\Omega}} \frac{\partial \hat{\varphi}_p}{\partial \hat{x}_2} \hat{\varphi}_i \hat{\varphi}_m d\hat{x} \right) \right] \\
 &+ \sum_{i,m=1}^{K(k)} \frac{g}{2 |\det(\mathbf{B}_e)|^{3/2}} c_{ei}^1 c_{em}^1 \left(B_{2,2}^e \int_{\hat{\Omega}} \frac{\partial \hat{\varphi}_p}{\partial \hat{x}_1} \hat{\varphi}_i \hat{\varphi}_m d\hat{x} - B_{2,1}^e \int_{\hat{\Omega}} \frac{\partial \hat{\varphi}_p}{\partial \hat{x}_2} \hat{\varphi}_i \hat{\varphi}_m d\hat{x} \right) \\
 &+ \sum_{i=1}^{K(k)} \frac{g h_b c_{ei}^1}{|\det(\mathbf{B}_e)|} \left(B_{2,2}^e \int_{\hat{\Omega}} \frac{\partial \hat{\varphi}_p}{\partial \hat{x}_1} \hat{\varphi}_i d\hat{x} - B_{2,1}^e \int_{\hat{\Omega}} \frac{\partial \hat{\varphi}_p}{\partial \hat{x}_2} \hat{\varphi}_i d\hat{x} \right) \tag{16}
 \end{aligned}$$

with a similar expression for $\phi_\Delta = \varphi_{ep} \mathbf{e}_3$ and rather trivial representations for element integrals arising from (12).

2.3 Mapping Math to Python

Since the quadrature-free formulation detailed above is a new element of our toolchain, it is a natural starting point for code generation. An abstract representation for the terms should be, on the one hand, as close as possible to the mathematical expression and, on the other, easy to transform to an efficient code. Another requirement is that the format or used environment of the abstract representation is accepted by its users. To meet all these requirements we have chosen to use `sympy`² within Python as the starting point. Python is one of the most often used languages currently, and `sympy` is a symbolic algebra package in Python with a rich functionality. Our new Python module to transform the DG scheme from a symbolic `sympy` expression into ExaSlang is called GHODDESS (Generation of Higher-Order Discretizations Deployed as ExaSlang Specifications). To generate code for the quadrature-free DG scheme, basic abstractions for, e.g., the basis functions have been implemented in GHODDESS just as classes representing triangles and data fields. Currently, we support quadrilateral grids only, where each element is divided into two differently oriented triangles in order to obtain a triangular grid. These special grids are obtained from our grid generator. The algebraic representations of the discrete scheme shown in Sec. 2.2 for element, edge, and boundary integrals are formulated in `sympy`. As an example consider the first part of element integral for ξ from (15):

$$\sum_{i=1}^{K(k)} \frac{c_{ei}^2}{|\det(\mathbf{B}_e)|} \left(B_{2,2}^e \int_{\hat{\Omega}} \frac{\partial \hat{\varphi}_p}{\partial \hat{x}_1} \hat{\varphi}_i d\hat{x} - B_{2,1}^e \int_{\hat{\Omega}} \frac{\partial \hat{\varphi}_p}{\partial \hat{x}_2} \hat{\varphi}_i d\hat{x} \right) \tag{17}$$

that is translated to

Listing 1: Part of element integral in Python representation.

```

sum(cu(tri.orientation, k) / tri.detB * (
    tri.B[1, 1] * sp.integrate(sp.Derivative(basisFcts[p], x, 1)
        * basisFcts[k], (y, 0, 1 - x), (x, 0, 1))
    - tri.B[1, 0] * sp.integrate(sp.Derivative(basisFcts[p], y, 1)
        * basisFcts[k], (y, 0, 1 - x), (x, 0, 1)))
    for k in range(d))

```

Information about the triangles such as the orientation or the determinant of the mapping from the reference triangle are stored in an object `tri`. `Sympy` is then used to evaluate integrals analytically which also allows us to perform symbolic algebra transforms on the integrals.

²<https://www.sympy.org/>

2.4 Mapping Python to ExaSlang

To allow a mapping from the symbolic representation to ExaSlang, sympy expressions are enriched with a few required abstractions such as field symbols that correspond to accesses to ExaSlang fields that store quantities defined on the computational domain. GHODDESS then maps to an auxiliary knowledge file holding parameters that guide the generation process as well as ExaSlang specifications on layer 3 and 4. The bulk part is emitted to layer 4 where the setup and solver phase are implemented. More information on the ExaSlang concept and its layers can be found in [28, 18]. For higher orders DG approximations, the layer 4 file can easily grow to several MB in size and take more than one hour to generate. The main reason for that is the quadrature-free scheme which involves symbolic integral evaluations and the complete unrolling of all loops, e.g., over basis functions. With increasing order of the DG method, the size of the expressions increases cubically in the number of local basis functions. Thus, one easily ends up with several million nodes in the abstract syntax tree (AST) resulting in a noticeable slow-down of the code transforms.

2.5 Mapping ExaSlang to Code

The ExaStencils code generator is then capable of parsing the ExaSlang code, applying transforms for certain low-level optimizations on the resulting AST and pretty-printing to C++ or CUDA code combined with MPI for distributed memory architectures. Currently, both the ExaStencils code generator and the C++ compiler, e.g., gcc take more than one hour for higher order DG discretizations due to the large size of the expressions – as described before. The overall runtime of a simulation can be in a similar range depending on the size of the computational grid and the order of the discretization. However, larger grids do not require more time for the code generation. Strategies to speed up the overall workflow are a part of our ongoing work.

3 Numerical results

Our implementation of the shallow water equations is planned to include an integrated generator for block-structured meshes. Since this functionality is still in a standalone testing stage, the grids employed for the runs in the current section are generated externally and read at runtime.

The main goal of the following numerical studies is to verify the implementation and to demonstrate the performance of our quadrature-free formulation for a range of benchmarks with analytically specified solutions.

3.1 Convergence test on a randomly perturbed regular mesh

For the first test, a rectangular domain $\Omega = [0 \pm r, 1000 \pm r] \times [0 \pm r, 1000 \pm r]$ is used, where r is a randomly generated perturbation of up to 20% of the edge length (cf. Fig. 3). The artificially manufactured analytical solution is given by

$$\begin{aligned}\xi(\mathbf{x}, t) &= 2 + y_a - 2 C_a \sin\left(\frac{\pi(x_0 + x_1 + C_t t)}{600}\right), \\ U(\mathbf{x}, t) &= 2 y_a + C_a C_t \sin\left(\frac{\pi(x_0 + x_1 + C_t t)}{600}\right), \\ V(\mathbf{x}, t) &= y_a + C_a C_t \sin\left(\frac{\pi(x_0 + x_1 + C_t t)}{600}\right)\end{aligned}$$

with the bathymetry specified as

$$h_b = 1 + \frac{1}{1000}x_0 + \frac{2}{1000}x_1$$

and suitable initial and Dirichlet boundary conditions. Simulations were run for $t \in (0, 1500)$ with the time step $\Delta t = 0.5$ chosen small enough to make the time discretization errors negligible compared to those of the spatial discretization. The remaining parameters are chosen as follows: $C_a = 0.2$, $C_t = 0.2$, $y_a = 0.3$.

Fig. 3 illustrates the mesh and the initial condition (left) and shows the final solution on the coarsest (level-2, middle) and finest (level-6, right) meshes for the piecewise linear (k=1) DG discretization. The errors for DG discretization spaces ranging from piecewise constants (k=0) to piecewise cubics (k=3) and the corresponding experimental convergence rates are listed in Tab. 1 and plotted in Fig. 4. The expected convergence rates are demonstrated for all primary unknowns (surface elevation and depth integrated velocity components) and the results are consistent with those presented in [1]. Due to increasing computational (and code generation) costs, runs for higher order DG discretizations stop at coarser mesh resolutions than the low order runs; nevertheless, the L^2 -errors for higher order approximations are much lower.

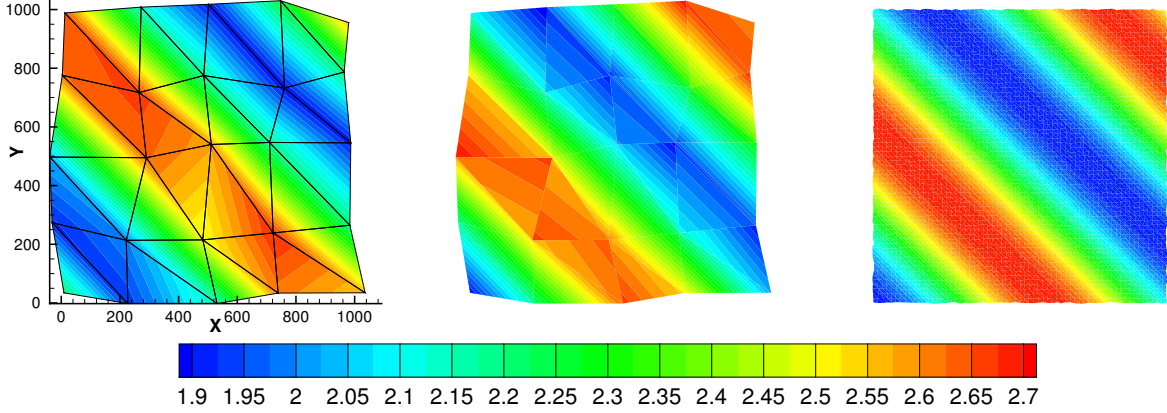


Figure 3: Square domain with perturbed mesh and piecewise linear ($k=1$) DG discretization: Level-2 mesh and the initial condition (left), final solution on the level-2 mesh (middle), final solution on the level-6 mesh (right).

DG order (k)	# elements	$\text{Err}(\xi)$	$\text{EOC}(\xi)$	$\text{Err}(U)$	$\text{EOC}(U)$	$\text{Err}(V)$	$\text{EOC}(V)$
0	32	141.24	-	88.049	-	96.451	-
	128	75.619	0.90	62.621	0.49	64.906	0.57
	512	38.070	0.99	35.016	0.84	35.753	0.86
	2048	19.093	1.00	18.458	0.92	18.953	0.92
	8192	9.5399	1.00	9.4733	0.96	9.7749	0.96
	32768	4.7698	1.00	4.7945	0.98	4.9692	0.98
1	32	45.085	-	123.68	-	101.33	-
	128	10.949	2.04	20.386	2.60	19.396	2.39
	512	2.6693	2.04	6.2844	1.70	5.4303	1.84
	2048	0.6760	1.98	1.2573	2.32	1.2092	2.17
	8192	0.1674	2.01	0.2651	2.25	0.2411	2.33
2	32	6.4361	-	14.090	-	21.492	-
	128	0.9973	2.69	2.1901	2.69	2.5439	3.08
	512	0.1239	3.01	0.2579	3.09	0.2419	3.39
	2048	0.0157	2.98	0.0263	3.29	0.0225	3.43
3	32	0.9669	-	1.8941	-	2.6533	-
	128	0.0608	3.99	0.0985	4.27	0.1167	4.51
	512	0.0036	4.08	0.0077	3.68	0.0069	4.07
	2048	0.0002	3.88	0.0004	4.15	0.0004	4.23

Table 1: L^2 -errors $\text{Err}(\cdot)$ and experimental orders of convergence $\text{EOC}(\cdot)$ for the square domain with perturbed mesh and DG discretization orders $k = 0, 1, 2, 3$.

3.2 Circular domain

The second test problem uses the same analytical solution as the previous one, but the domain is now ring-shaped with the inner radius of 500, outer radius of 1000, and centered at the origin. The ring is divided into 8 patches corresponding to MPI ranks. Fig. 5 shows the coarsest mesh with the initial condition (left), the final solution on the coarsest mesh (level-2, middle), and the final solution on the finest mesh (level-6, right) for the piecewise linear ($k=1$) DG discretization.

4 Conclusion and Outlook

This work introduced for the first time quadrature-free functionality for a SWE model based on the discontinuous Galerkin discretization. In the future work, we'll demonstrate the performance of this methodology using simulations of real-life problems on complex 2D domains and test its scalability and computational performance on a range of different hardware architectures. Furthermore, we plan to transfer our approaches to 3D coastal ocean models such as implemented in UTBEST3D [14, 4, 26].

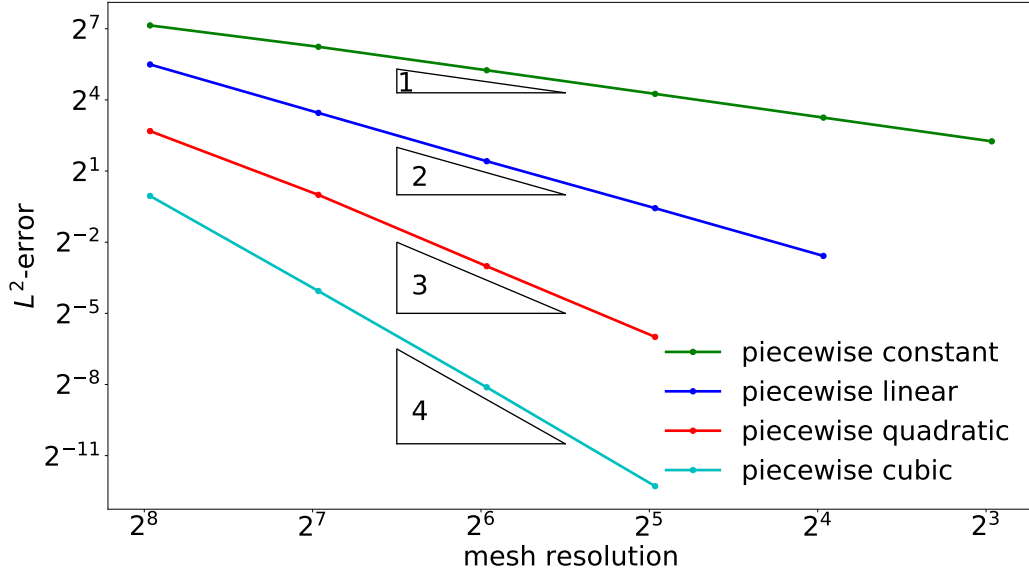


Figure 4: L^2 -errors for ξ vs. the mesh resolution (cell width of the unperturbed mesh).

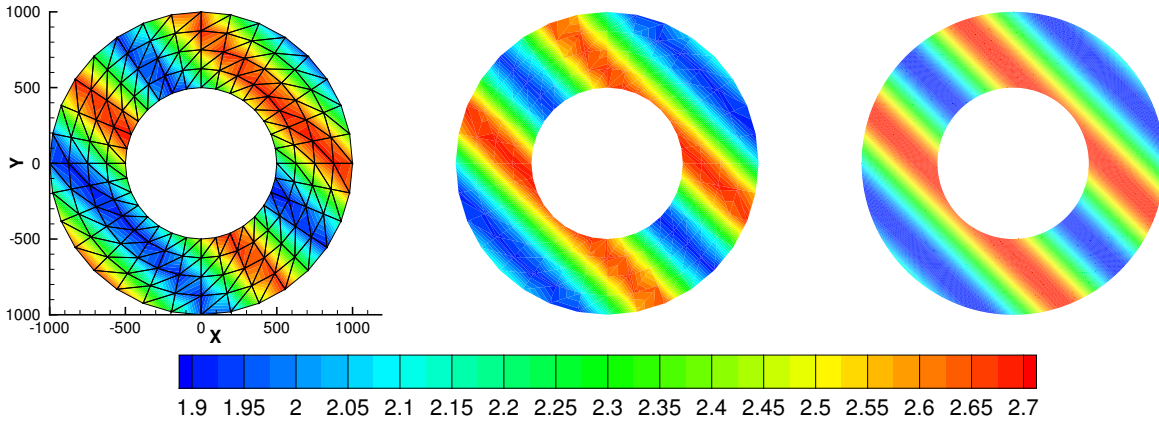


Figure 5: Circular domain and piecewise linear ($k=1$) DG discretization: Level-2 mesh and the initial condition (left), final solution on the level-2 mesh (middle), final solution on the level-6 mesh (right).

To complete the code generation pipeline, we plan to provide and incorporate the UFL (unified form language) similarly to approaches used in other code generation frameworks as abstract representation on layer 1. In addition to that, full support for block-structured grids should be available soon. We currently also work on improving node-level performance and scalability.

Acknowledgements

The authors acknowledge financial support by the German Research Foundation (DFG) through grants AI 117/6-1, KO 4641/1-1, and GR 1107/3-1.

References

- [1] V. Aizinger. *A Discontinuous Galerkin Method for Two- and Three-Dimensional Shallow-Water Equations*. PhD thesis, University of Texas at Austin, 2004.
- [2] V. Aizinger, L. Bungert, and M. Fried. Comparison of two local discontinuous Galerkin formulations for the subjective surfaces problem. *Computing and Visualization in Science*, 18(6):193–202, 2018.

- [3] V. Aizinger and C. Dawson. A discontinuous Galerkin method for two-dimensional flow and transport in shallow water. *Adv Water Resour.*, 25(1):67–84, 2002.
- [4] V. Aizinger, J. Proft, C. Dawson, D. Pothina, and S. Negusse. A three-dimensional discontinuous Galerkin model applied to the baroclinic simulation of Corpus Christi Bay. *Ocean Dynamics*, 63(1):89113, 2013.
- [5] M. S. Alnæs, A. Logg, K. B. Ølgaard, M. E. Rognes, and G. N. Wells. Unified form language: A domain-specific language for weak formulations of partial differential equations. *ACM Trans. on Mathematical Software (TOMS)*, 40(2):9:1–9:37, 2014.
- [6] M. Asai, Y. Miyagawa, N. Idris, A. Muhari, and F. Imamura. Coupled tsunami simulations based on a 2d shallow-water equation-based finite difference method and 3d incompressible smoothed particle hydrodynamics. *Journal of Earthquake and Tsunami*, 10(05), 2016.
- [7] H.L. Atkins and C.-W. Shu. Quadrature-free implementation of discontinuous Galerkin method for hyperbolic equations. *AIAA Journal*, 36(5):775–782, 1998.
- [8] M. Bader, C. Böck, J. Schwaiger, and C. Vigh. Dynamically adaptive simulations with minimal memory requirements solving the shallow water equations using Sierpinski curves. *SIAM Journal on Scientific Computing*, 32(1):212–228, 2010.
- [9] A. O. Bankole, A. Iske, T. Rung, and M. Dumbser. A semi-implicit SPH scheme for the two-dimensional shallow water equations. In *Proceedings of the 10th International SPHERIC Workshop, Parma, Italy*, pages 252–258, 2015.
- [10] L. Bungert, V. Aizinger, and M. Fried. A discontinuous Galerkin method for the subjective surfaces problem. *Journal of Mathematical Imaging and Vision*, 58(1):147161, 2017.
- [11] V. Casulli. Semi-implicit finite difference methods for the two-dimensional shallow water equations. *Journal of Computational Physics*, 86(1):56–74, 1990.
- [12] B. Cockburn and C. Shu. The local discontinuous Galerkin method for time-dependent convection–diffusion systems. *SIAM Journal on Numerical Analysis*, 35(6):2440–2463, 1998.
- [13] C. Dawson and V. Aizinger. The local discontinuous Galerkin method for advection-diffusion equations arising in groundwater and surface water applications. In J. Chadam, A. Cunningham, R. E. Ewing, P. Ortoleva, and M. F. Wheeler, editors, *Resource Recovery, Confinement, and Remediation of Environmental Hazards*, page 231245. Springer, 2002.
- [14] C. Dawson and V. Aizinger. A discontinuous Galerkin method for three-dimensional shallow water equations. *Journal of Scientific Computing*, 22(1-3):245267, 2005.
- [15] M. Dubiner. Spectral methods on triangles and other domains. *Journal of Scientific Computing*, 6(4):345–390, Dec 1991.
- [16] T. Gysi, C. Osuna, O. Fuhrer, M. Bianco, and T. C. Schulthess. STELLA: A domain-specific tool for structured grid methods in weather and climate models. In *Proceedings of International Conference for High Performance Computing, Networking, Storage and Analysis (SC)*, pages 41:1–41:12. ACM, nov 2015.
- [17] H. Hajduk, B. R. Hodges, V. Aizinger, and B. Reuter. Locally Filtered Transport for computational efficiency in multi-component advection-reaction models. *Environmental Modelling & Software*, 102:185–198, 2018.
- [18] S. Kuckuk and H. Köstler. Whole program generation of massively parallel shallow water equation solvers. In *2018 IEEE International Conference on Cluster Computing (CLUSTER)*, pages 78–87. IEEE, 2018.
- [19] W. Lai and A. A. Khan. A parallel two-dimensional discontinuous Galerkin method for shallow-water flows using high-resolution unstructured meshes. *Journal of Computing in Civil Engineering*, 31(3), 2016.
- [20] P.-W. Li and C.-M. Fan. Generalized finite difference method for two-dimensional shallow water equations. *Engineering Analysis with Boundary Elements*, 80:58–71, 2017.
- [21] D. Lockard and H. Atkins. Efficient implementations of the quadrature-free discontinuous Galerkin method. In *Proceeding of 14th AIAA CFD conference*. AIAA, pages 526–536, 1999.
- [22] A. Logg, K.-A. Mardal, and G. N. Wells. *Automated Solution of Differential Equations by the Finite Element Method*, volume 84 of *Lecture Notes in Computational Science and Engineering (LNCSE)*. Springer, 2012.
- [23] A. Pöppel and M. Bader. Swe-x10: An actor-based and locally coordinated solver for the shallow water equations. In *Proceedings of the 6th ACM SIGPLAN Workshop on X10*, pages 30–31. ACM, 2016.
- [24] M. Püschel, F. Franchetti, and Y. Voronenko. *Spiral*, volume 4, pages 1920–1933. Springer, 2011.

- [25] F. Rathgeber, D. A. Ham, L. Mitchell, M. Lange, F. Luporini, A. T. T. Mcrae, G.-T. Bercea, G. R. Markall, and P. H. J. Kelly. Firedrake: Automating the finite element method by composing abstractions. *ACM Trans. on Mathematical Software (TOMS)*, 43(3):24:1–24:27, 2016.
- [26] B. Reuter, V. Aizinger, and H. Köstler. A multi-platform scaling study for an openmp parallelization of a discontinuous Galerkin ocean model. *Computers and Fluids*, 117:325 – 335, 2015.
- [27] C. Schmitt, S. Kronawitter, F. Hannig, J. Teich, and C. Lengauer. Automating the development of high-performance multigrid solvers. In *Proc. of the IEEE*, 2018. Special Issue From High Level Specification to High Performance Code; to appear.
- [28] Christian Schmitt, S. Kuckuk, F. Hannig, H. Köstler, and J. Teich. Exaslang: a domain-specific language for highly scalable multigrid solvers. In *Domain-Specific Languages and High-Level Frameworks for High Performance Computing (WOLFHPC), 2014 Fourth International Workshop on*, pages 42–51. IEEE, 2014.
- [29] D. Unat, X. Cai, and S. B. Baden. Mint: Realizing CUDA performance in 3d stencil methods with annotated C. In *Proceedings of International Conference on Supercomputing (ICS)*, pages 214–224. ACM, jun 2011.
- [30] R. Vacondio, A. Dal Palù, A. Ferrari, P. Mignosa, F. Aureli, and S. Dazzi. A non-uniform efficient grid type for GPU-parallel shallow water equations models. *Environmental Modelling & Software*, 88:119–137, 2017.
- [31] T. Weinzierl, M. Bader, K. Unterweger, and R. Wittmann. Block fusion on dynamically adaptive spacetime grids for shallow water waves. *Parallel Processing Letters*, 24(03), 2014.
- [32] N. Wintermeyer, A. R. Winters, G. J. Gassner, and D. A. Kopriva. An entropy stable nodal discontinuous Galerkin method for the two dimensional shallow water equations on unstructured curvilinear meshes with discontinuous bathymetry. *Journal of Computational Physics*, 340:200–242, 2017.
- [33] R. Wittmann, H.-J. Bungartz, and P. Neumann. High performance shallow water kernels for parallel overland flow simulations based on FullSWOF2D. *Computers & Mathematics with Applications*, 74(1):110–125, 2017.
- [34] D. Zint, R. Grosso, V. Aizinger, and H. Köstler. Generation of block structured grids on complex domains for high performance simulation (accepted). In *Proceedings of the 9th International Conference on Numerical Geometry, Grid Generation and Scientific Computing (NUMGRID2018)*, 2018.